

Mollow triplet: pump probe single photon spectroscopy of artificial atoms

Ya. S. Greenberg^{1,*} and A. N. Sultanov^{1,†}

¹*Novosibirsk State Technical University, Novosibirsk, Russia*

(Dated: April 9, 2019)

We analyze a photon transport through an 1D open waveguide side coupled to the N -photon microwave cavity with embedded artificial atom (qubit). The qubit state is probed by a weak signal at the fundamental frequency of the waveguide. Within the formalism of projection operators and non-Hermitian Hamiltonian approach we develop a one-photon approximation scheme for the calculation of the probability amplitudes of the spontaneous transitions between the levels of two Rabi doublets in N - photon cavity. We obtain analytic expressions for the transmission and reflection factors of the microwave signal through a waveguide, which contain the information of the qubit parameters. We show that for small number of cavity photons the Mollow spectrum consists of four spectral lines which is a direct manifestation of quantum nature of light. The results obtained in the paper are of general nature and can be applied to any type of qubits. The specific properties of the qubit are only encoded in the two parameters: the energy Ω of the qubit and its coupling λ to the cavity photons.

PACS numbers: 42.50.Ct, 42.50.Dv, 42.50.Pq

I. INTRODUCTION

The coherent coupling of a superconducting qubit to the microwave modes of a 1D coplanar waveguide transmission line has been intensely investigated over the last years both experimentally and theoretically. As compared with the conventional optical cavity with atomic gases, superconducting qubits as artificial atoms in solid-state devices have significant advantages, such as technological scalability, long coherence time which is important for the implementation of the quantum gate operations, huge tunability and controllability by external electromagnetic fields [1–4]. Another advantage is an on-chip realization of strong and ultrastrong coupling regimes [5, 6] previously inaccessible to atomic systems. This enables us to explore novel quantum phenomena emerging only in this regime. Furthermore, solid state superconducting circuits with embedded Josephson junction qubits have reproduced many physical phenomena known previously from quantum optics, such as Kerr nonlinearities [7, 8], electromagnetically induced transparency [9–12], the Mollow triplet [13–17], and Autler-Townes splitting [9, 13, 18].

As the Mollow triplet is a clear manifestation of the coherent nature of the light- matter interaction, its fluorescent or transmission spectra can be explained considering the pumping light classically [19]. Instead of looking at the emission fluorescent spectrum we study here the transmission of a single photon which induces the transitions in a preliminary pumped cavity. The use of a single photon source as a probe reveals a marked influence of the quantum nature of light on the Mollow spectra and allows us to determine the response to the input of a single injected photon [16, 17, 20]. Thus, a theoretical framework that allows one to directly calculate the response of such a system to a single injected photon is justified.

In the present paper we consider the transmission and re-

flection Mollow spectra for artificial atom (qubit) embedded in the N - photon cavity which is side- coupled to open microwave waveguide.

Our analysis is based on the projection operators formalism and the method of the effective non- Hermitian Hamiltonian which has many applications for different open mesoscopic systems (see review paper [21] and references therein). Recently this method has been applied to photon transport through 1D open transmission line with N embedded qubits [22].

A principle motivation for this research is to obtain analytic solution for the scattering of a single photon on N - photon cavity with embedded qubit where the cavity is coupled to open transmission line. For $N = 1$ this problem can be solved by several methods [23, 24]. For $N > 1$ the solution of master equation for the density matrix can be obtained only by numerical integration of a truncated set of Bloch- like equations of motions for the expectation values of the qubit and photon operators and their different products [25]. As to our knowledge, even for $N = 2$ the analytic expressions for photon transport coefficients are not known.

The results obtained in the paper are relevant for the experiments where a qubit+cavity system is preliminary being driven by a fixed-frequency pump field to one of its excited N - photon states, with transitions to higher-lying states being studied by a weak, variable-frequency single photon probe [20].

We find the analytic expressions for the probability amplitudes of the spontaneous transitions induced by injected photon in N - photon cavity. This enables us to find the forms of spectral lines depending on the qubit parameters and on the number of photons in a cavity. We show that for small number of cavity photons the transmission and reflection spectra consist of four lines which is a direct manifestation of quantum nature of light. As the number of cavity photons is increased two central peaks merge giving a conventional Mollow triplet.

The paper is organized as follows. In Sec.II we briefly describe the projection operators formalism and the method of effective non hermitian Hamiltonian. In Sec.III we define the Hamiltonian of 1D waveguide side coupled to the N - pho-

*Electronic address: greenberg@risc.ru

†Electronic address: sultanov.aydar@ngs.ru

ton microwave cavity with embedded qubit and qualitatively describe the process of a single photon scattering. The analytical expression for the effective non-hermitian Hamiltonian is given in Sec.IV. In this section we find the spectrum of the cavity resonances and their dependence on the cavity decay rate Γ , cavity-qubit coupling strength λ and the number of cavity photons N . The wave function of the scattering photon is found in Sec.V, where we obtain the explicit analytical expressions for the probability amplitudes which describe spontaneous transitions between the levels of two Rabi doublets. These amplitudes are directly related to the transmission and reflection factors and show representative photon spectra. The results obtained in Sec.V are applied in Sec.VI where we compare the transmission amplitudes for $N = 2$ with those for $N = 1$.

II. PROJECTION FORMALISM AND EFFECTIVE NON-HERMITIAN HAMILTONIAN

We start with a brief review of projection formalism, highlighting only those aspects that will be required for the paper here. The application of this method to photon transport was described in more detail in [22].

According to this method the Hilbert space of a quantum system with the Hermitian Hamiltonian H is formally subdivided into two arbitrarily selected orthogonal projectors, P and Q , which satisfy the following properties:

$$P + Q = 1; \quad PQ = QP = 0; \quad PP = P; \quad QQ = Q \quad (1)$$

Keeping in mind the scattering problem we assume that Q subspace determines a closed system and, therefore, consists of discrete states, and P subspace consists of the states from continuum. Those states of subspace Q which will turn out to be coupled to the states in subspace P will acquire the outgoing waves and become unstable. Then, for this scattering problem the effective Hamiltonian which describes the decay of Q - subsystem, becomes non Hermitian and has to be written as follows:

$$H_{eff}(E) = H_{QQ} + H_{QP} \frac{1}{E - H_{PP} + i\varepsilon} H_{PQ} \quad (2)$$

where $H_{XY} = XHY$, with X, Y being Q or P .

The effective Hamiltonian (2) determines the resonance energies of the Q - subsystem which are due to its interaction H_{PQ} with continuum states from P - system. These resonances lie in the low half of the complex energy plane, $z = \tilde{E} - i\hbar\tilde{\Gamma}$ and are given by the roots of the equation

$$D(z) \equiv \det(z - H_{eff}) = 0 \quad (3)$$

The imaginary part $\tilde{\Gamma}$ of the resonances describes the decay of Q - states due to their interaction with continuum P - states.

The scattering solution for the state vector of the Shrödinger equation $H\Psi = E\Psi$ reads [26]

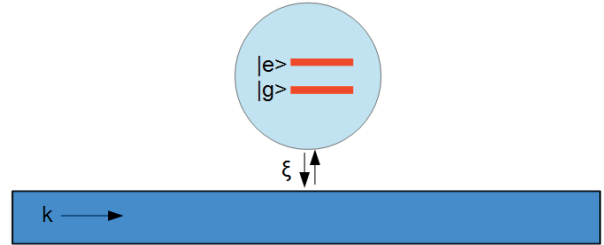


FIG. 1: (Color online) Waveguide side coupled to the N - photon cavity with imbedded qubit

$$\begin{aligned} |\Psi\rangle = & |in\rangle + \frac{1}{E - H_{eff}} H_{QP} |in\rangle \\ & + \frac{1}{E - H_{PP} + i\varepsilon} H_{PQ} \frac{1}{E - H_{eff}} H_{QP} |in\rangle \end{aligned} \quad (4)$$

where $|in\rangle$ is the initial state, which contains continuum variables and satisfies the equation $H_{PP}|in\rangle = E|in\rangle$.

The last term in the expression (4) describes to all orders of H_{QP} the evolution of initial state $|in\rangle$ under the interaction between P and Q subspaces.

It is useful to stress that the formal results (2) and (4) do not require any explicit expressions for the projection operators.

III. SINGLE PHOTON SCATTERING

We consider a microwave 1D waveguide side coupled to a cavity with embedded qubit as is shown in Fig.1.

The Hamiltonian of the system reads:

$$\begin{aligned} H = & \sum_k \hbar\omega_k c_k^+ c_k + \frac{1}{2} \hbar\Omega\sigma_z + \hbar\omega_c a^+ a + \hbar\lambda(a^+ + a)\sigma_x \\ & + \hbar\xi \sum_k (c_k^+ a + c_k a^+) \end{aligned} \quad (5)$$

where the first three terms are, respectively the Hamiltonian of waveguide photons, the Hamiltonian of the qubit with the excitation frequency Ω , the Hamiltonian of one mode cavity. Fourth and fifth terms describe the qubit-cavity interaction with the strength λ , and the interaction between the waveguide and the cavity with the strength ξ .

As we study a single photon probe we assume that at every instant there is either one photon in a waveguide and $N - 1$ photons in a cavity or no photons in a waveguide and N photons in a cavity. Therefore, we assume that our Hilbert space is restricted to the following state vectors:

$$|1\rangle \equiv |0\rangle \otimes |N, g\rangle, \quad |2\rangle \equiv |0\rangle \otimes |N - 1, e\rangle \quad (6)$$

$$|k_1\rangle \equiv |k\rangle \otimes |N - 1, g\rangle, \quad |k_2\rangle \equiv |k\rangle \otimes |N - 2, e\rangle \quad (7)$$

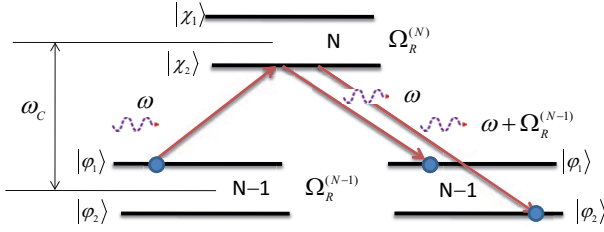


FIG. 2: Color online. A scheme of a scattering of a single photon on the state $|\varphi_1\rangle$ of $(N-1)$ -cavity when the transition $|\varphi_1\rangle \rightarrow |\chi_2\rangle$ is excited.

The states (6) correspond to no photons in a waveguide, N photons in the cavity, and a qubit in the ground g or excited state e . The states (7) correspond to the situation where one photon with a momentum k is in a waveguide, $N-1$ photons in the cavity, and a qubit in the ground g or excited state e .

Due to the interaction between cavity photons and a qubit each of the pair of states (6) and (7) are being hybridized to two pairs of dressed states $|\chi_{i,0}\rangle = |0\rangle \otimes |\chi_i\rangle$, $|\varphi_{i,k}\rangle = |k\rangle \otimes |\varphi_i\rangle$, where

$$|\chi_i\rangle = \alpha_i|N, g\rangle + \beta_i|N-1, e\rangle \quad (8)$$

$$|\varphi_i\rangle = a_i|N-1, g\rangle + b_i|N-2, e\rangle \quad (9)$$

Every pair of these dressed states are split by a Rabi frequency corresponding to the number of the cavity photons:

$$\Omega_R^{(N)} = \sqrt{\Delta^2 + 4\lambda^2 N} \quad (10)$$

For subsequent calculations we need only the explicit form of the superposition factors a_i and b_i in (9) which can be expressed in terms of the angle variable θ : $\tan 2\theta = -2\lambda(N-1)/\Delta$ with $a_1 = b_2 = \sin \theta$, $b_1 = -a_2 = \cos \theta$.

The process of the photon scattering can be qualitatively described as follows. Before a probing photon enters a waveguide the $N-1$ photon cavity + qubit system is in one of its hybridized states $|\varphi_i\rangle$ ($i = 1, 2$) (9) that was prepared by a preliminary pumping. The multiple interaction of a probing photon with a cavity leads to the formation of quasienergy hybridized states (8). These states subsequently decay with one photon being escaped to a waveguide, and a cavity + qubit system being left in one of the states (9). This picture is illustrated in Fig. 2 where the incoming photon excites the $|\varphi_1\rangle$ state to the state $|\chi_2\rangle$ at the frequency $\omega = \omega_C - \frac{1}{2}(\Omega_R^{(N)} + \Omega_R^{(N-1)})$. The state $|\chi_2\rangle$ subsequently decays either to the initial state $|\varphi_1\rangle$ with the outgoing photon having the excitation frequency ω or to the state $|\varphi_2\rangle$ with the outgoing photon having the frequency $\omega + \Omega_R^{(N-1)}$.

Hence there four possible outcomes of a probing photon scattering depending on which of the two states (9) were prepared by a preliminary pumping. These four possible channels are shown in Fig.3.

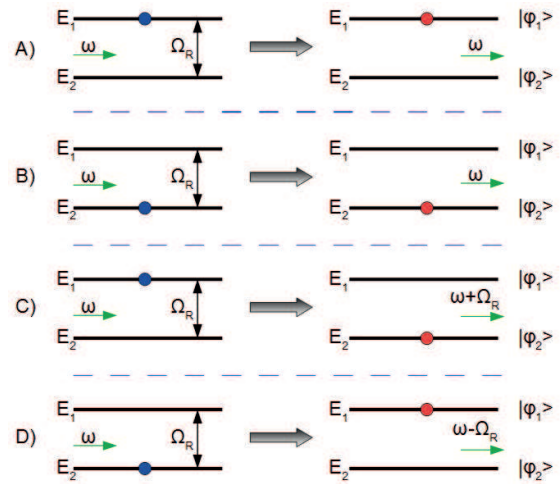


FIG. 3: (Color online) Four outcomes of the scattering process. Two upper graphs correspond to elastic scattering, while two lower graphs correspond to inelastic sidebands. Blue circles denote the initial state, red ones denote the final state.

Two channels describe the elastic scattering when the initial and final states of the $N-1$ cavity + qubit system before and after scattering are the same, and the energies of incoming and outgoing photons are equal. The other two channels describe inelastic process when the outgoing photon gains or loses its energy by amount of $\hbar\Omega_R^{(N-1)}$. Every channel shown in Fig.3 corresponds to a specific transmission factor that will be calculated below. Each channel has two resonances which correspond to two transitions from N photon cavity to one of the final states φ_i . For example, the channel A in Fig.3 has one resonance at the frequency $\omega = \omega_C - \frac{1}{2}(\Omega_R^{(N)} + \Omega_R^{(N-1)})$ that induces the transition $|\varphi_1\rangle \rightarrow |\chi_2\rangle$ (see Fig.2). The other resonance is at the frequency $\omega = \omega_C + \frac{1}{2}(\Omega_R^{(N)} - \Omega_R^{(N-1)})$ that induces the transition $|\varphi_1\rangle \rightarrow |\chi_1\rangle$. Each of these resonances subsequently decays to the initial state $|\varphi_1\rangle$.

IV. CAVITY RESONANCES

In accordance with the projection operators formalism we define two mutual orthogonal subspaces as follows

$$Q = |1\rangle\langle 1| + |2\rangle\langle 2| \quad (11)$$

$$P = \sum_k \sum_{n=1}^2 |k_n\rangle\langle k_n| = \frac{L}{2\pi} \int dk \sum_{n=1}^2 |k_n\rangle\langle k_n| \quad (12)$$

where L is the length of waveguide, and the orthogonality condition for P subspace vectors is

$$\langle k_n | k'_m \rangle = \frac{2\pi}{L} \delta_{n,m} \delta(k_n - k'_m) \quad (13)$$

where $n, m = 1, 2$.

The application of the method requires the continuum state vectors to be the eigenfunctions of Hamiltonian H_{PP} . This is not the case for (7) since H_{PP} couples two vectors $|k_1\rangle$ and $|k_2\rangle$. It is not difficult to show that the state vectors $|\varphi_{i,k}\rangle$ defined in (9), are the eigenfunctions of H_{PP} with the energies

$$E_i/\hbar = -\frac{1}{2}\omega_c + \omega_c(N-1) + \omega - \frac{1}{2}(-1)^i\Omega_R^{(N-1)} \quad (14)$$

where ω is the frequency of incident photon.

The matrix elements of H_{eff} in the Q subspace is as follows

$$\langle 1|H_{eff}|1\rangle = \omega_C N - \frac{1}{2}\Omega - jN\Gamma \quad (15a)$$

$$\langle 2|H_{eff}|2\rangle = \omega_C(N-1) + \frac{1}{2}\Omega - j(N-1)\Gamma \quad (15b)$$

$$\langle 1|H_{eff}|2\rangle = \langle 2|H_{eff}|1\rangle = \lambda\sqrt{N} \quad (15c)$$

where we introduce the width of the cavity decay rate $\Gamma = L\xi^2/v_g$. The details of the calculation of Eqs. 15a, 15b, 15c are given in the Appendix B.

Due to the interaction of the Q states (6) with continuum states (7) the former acquire the resonances whose energies and widths become dependent on the coupling parameter ξ in Hamiltonian (5), which defines the width of the cavity decay rate Γ . These resonances are given by the complex roots of Eq.3. For H_{eff} given by the matrix elements (15a), (15b), (15c) this equation reads:

$$D(z) = \left(z/\hbar + \frac{1}{2}\Omega - \omega_c N + jN\Gamma \right) \times \left(z/\hbar - \frac{1}{2}\Omega - \omega_c(N-1) + j(N-1)\Gamma \right) - \lambda^2 N = 0 \quad (16)$$

where the complex energy z is given by (14) where the frequency of incident photon ω is replaced by the complex value $\tilde{\omega}$.

Every of two Q states (6) may decay in two ways: either to the state $|\varphi_{1,k}\rangle$ with the energy E_1 or to the state $|\varphi_{2,k}\rangle$ with the energy E_2 .

Accordingly, in both cases ($i = 1, 2$) we obtain:

$$D(E_i) = (\omega - \tilde{\omega}_{i+})(\omega - \tilde{\omega}_{i-}) \quad (17)$$

where $\omega_{i\pm}$ are complex roots of the equation (16).

$$\tilde{\omega}_{1,\pm} = \omega_C - \frac{1}{2} \left[\Omega_R^{(N-1)} + j(2N-1)\Gamma \right] \pm \frac{1}{2} \sqrt{(\Delta - j\Gamma)^2 + 4\lambda^2 N} \quad (18a)$$

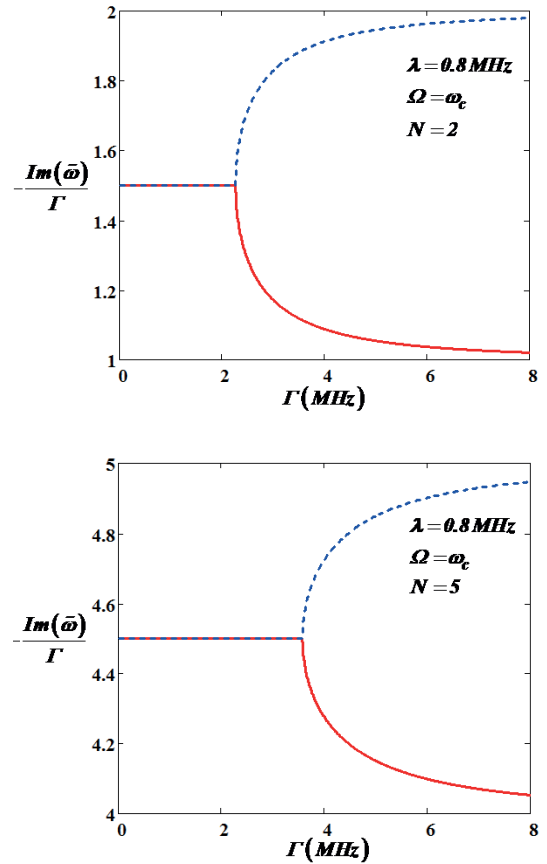


FIG. 4: (Color online) The dependence of the resonance widths on the cavity decay rate Γ for $\Delta = 0$. For $\Gamma < 2\lambda\sqrt{N}$ all widths are the same. The splitting starts at the point $\Gamma = 2\lambda\sqrt{N}$. Dashed (blue) line corresponds to $\tilde{\omega}_{1,-}, \tilde{\omega}_{2,-}$. Solid (red) line corresponds to $\tilde{\omega}_{1,+}, \tilde{\omega}_{2,+}$

$$\tilde{\omega}_{2,\pm} = \omega_C + \frac{1}{2} \left[\Omega_R^{(N-1)} - j(2N-1)\Gamma \right] \pm \frac{1}{2} \sqrt{(\Delta - j\Gamma)^2 + 4\lambda^2 N} \quad (18b)$$

Since $\tilde{\omega}_{2,\pm} = \tilde{\omega}_{1,\pm} + \Omega_R^{(N-1)}$, the dependence of real and imaginary part of these resonances on Γ is the same for both cases. The dependence of the resonance widths on Γ is shown in Fig.4 for $\Delta = 0$. The position of splitting corresponds to the point $2\lambda\sqrt{N} = \Gamma$.

The real parts of (18a), (18b) correspond to the energy spacing between the levels of two manifolds shown in Fig.2. The transitions $\varphi_1 \rightarrow \chi_2, \varphi_1 \rightarrow \chi_1, \varphi_2 \rightarrow \chi_2, \varphi_2 \rightarrow \chi_1$ correspond to $Re(\tilde{\omega}_{1-}), Re(\tilde{\omega}_{1+}), Re(\tilde{\omega}_{2-}), Re(\tilde{\omega}_{2+})$, respectively.

Figure 5 shows the dependence of resonance energies on Γ for $\Delta = 0$, where for $\Gamma > 2\lambda\sqrt{N}$ the resonance energies do not depend on Γ and shifted by $\Omega_R^{(N-1)}$. For $\Gamma < 2\lambda\sqrt{N}$ there exist all four resonances separately. For nonzero detuning Δ the widths are split for any Γ as shown in the upper plot of Fig.6. The real parts of resonance energies dis-

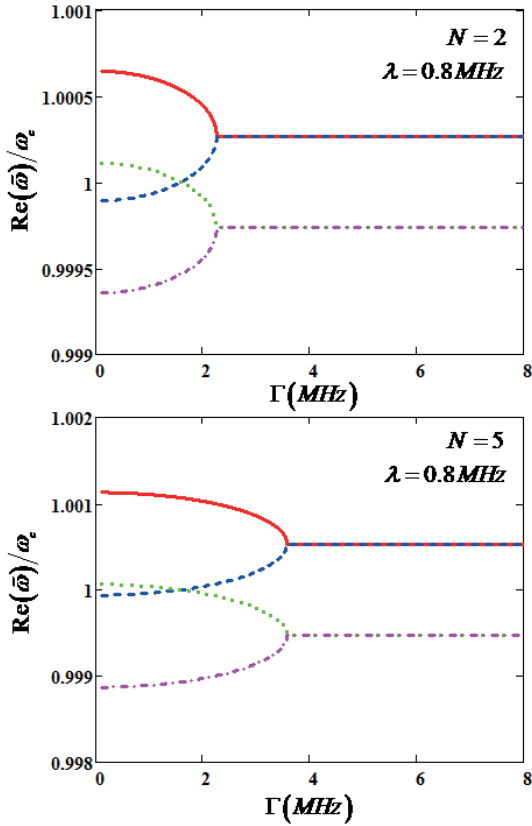


FIG. 5: (Color online) The dependence of resonance energy on Γ for $\Delta = 0$. Upper curve corresponds to $\tilde{\omega}_{2,\pm}$, the lower one- to $\tilde{\omega}_{1,\pm}$. For $\Gamma > 2\lambda\sqrt{N}$ the resonance energies do not depend on Γ and shifted by Ω_R . For $\Gamma < 2\lambda\sqrt{N}$ there exist all four resonances separately.

plays all four components as shown in the lower plot of Fig.6. The dependence of resonances on the photon number N for weak and strong coupling is shown in Fig.7 for zero frequency detuning $\Delta = 0$. From (18a), (18b) we can analyze the dependence of resonance frequencies on the coupling strength λ . For relatively small coupling $\lambda/\Gamma < 1/2\sqrt{N}$, $Re(\tilde{\omega}_{1+}) = Re(\tilde{\omega}_{1-})$ and $Re(\tilde{\omega}_{2+}) = Re(\tilde{\omega}_{2-})$. The splitting begins at the point $\lambda/\Gamma = 1/2\sqrt{N}$. As the ratio λ/Γ is further increased, the frequencies (18a), (18b) scale as follows: $Re(\tilde{\omega}_{1-}) \approx \omega_c - 2\lambda\sqrt{N}$, $Re(\tilde{\omega}_{2+}) \approx \omega_c + 2\lambda\sqrt{N}$, $Re(\tilde{\omega}_{1+}) \approx \omega_c + \lambda/2\sqrt{N}$, $Re(\tilde{\omega}_{2-}) \approx \omega_c - \lambda/2\sqrt{N}$. These features are shown in Fig. 8 for zero detuning and $N = 5$.

As we show in Sec.V, the transmission factors scales as $1/D(E_1)$ or $1/D(E_2)$. Therefore, the resonances of these quantities, which are given by the roots (18a) and (18b) reflects the intrinsic properties of the cavity-qubit system. We will see below that transmission and reflection factors are peaked at the energies which correspond to the real parts of (18a) and (18b).

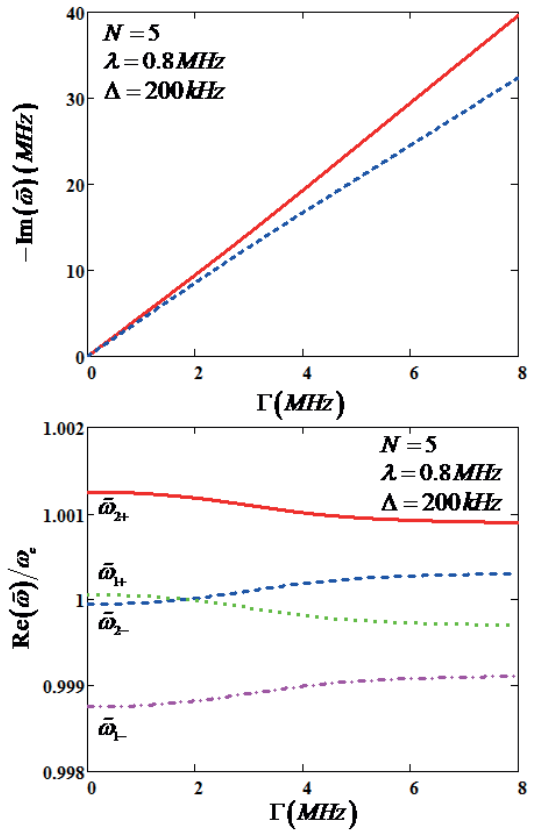


FIG. 6: (Color online) The dependence of imaginary (upper plot) and real (lower plot) parts of resonances on Γ for nonzero detuning. The solid (red) curve at upper plot corresponds to $\tilde{\omega}_{1,2+}$, while the dashed (blue) curve corresponds to $\tilde{\omega}_{1,2-}$.

V. THE WAVE FUNCTION OF THE SCATTERING PHOTON

The key notion for the subsequent calculation of photon transmission and reflection is a transmission matrix

$$\begin{aligned} & \langle j, k' | T | k, i \rangle \\ &= \sum_{n,m=1}^2 \langle \varphi_{j,k'} | H_{PQ} | n \rangle R_{n,m}(E_i) \langle m | H_{QP} | \varphi_{i,k} \rangle \end{aligned} \quad (19)$$

where the matrix $R_{m,n}(E) = (\langle m | (E - H_{eff}) | n \rangle)^{-1}$ is calculated in Appendix C.

In our case the transmission matrix (19) does not depend on the final momentum k' (detail are given in Appendix). The dependence of (19) on initial momentum k is hidden in the energies E_i (14), which depend on the frequency ω of incident photon.

The quantity (19) describes the process where the incident photon with momentum k comes into interaction with a cavity that was initially in the state $|\varphi_i\rangle$ and then escapes with momentum k' leaving the cavity in the state $|\varphi_j\rangle$. Therefore, four different outcomes of this scattering processes for transmitted

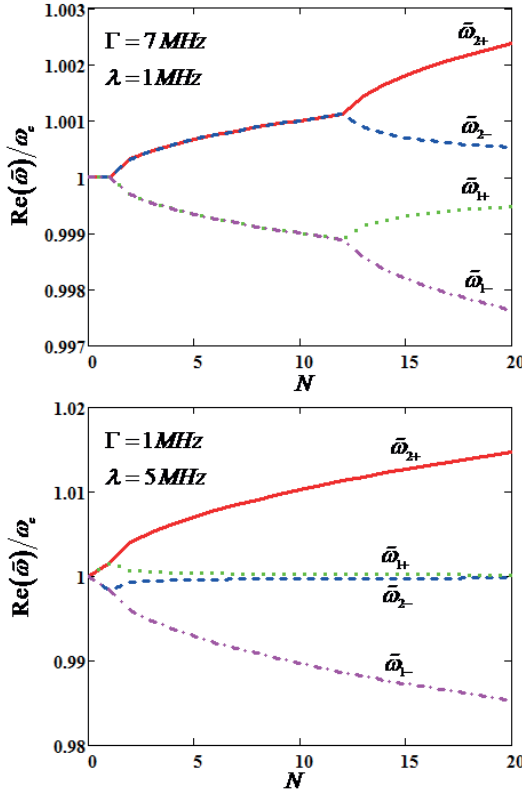


FIG. 7: (Color online) The dependence of real parts of $\tilde{\omega}_{1,\pm}$ and $\tilde{\omega}_{2,\pm}$ for weak (upper plot) and strong (lower plot) coupling on the photon number N for zero detuning.

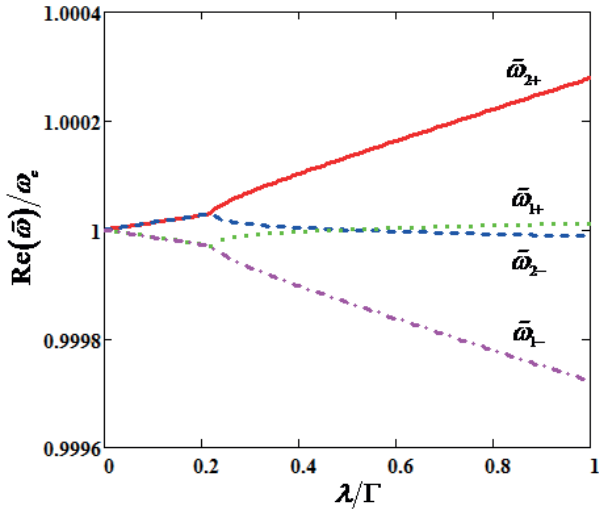


FIG. 8: (Color online) The dependence of the positions of the resonance peaks on the coupling strength between qubit and cavity photons for $\Delta = 0$ and $N = 5$.

probe signal are possible: two of them correspond to elastic scattering and two of them correspond to inelastic process with the momenta of outgoing photon $k' = k \pm \Omega_R^{(N-1)}/v_g$ (see Fig.3). According to these possibilities the initial state $|in\rangle$ in (4) corresponds to either $|\varphi_{1,k}\rangle$ or $|\varphi_{2,k}\rangle$.

$$|\Psi_1\rangle = |\varphi_{1,k}\rangle + \sum_{m,n} |n\rangle R_{nm}(E_1) \langle m| H_{QP} |\varphi_{1,k}\rangle + \sum_{q,i} \frac{|\varphi_{i,q}\rangle}{E_1(k) - E_i(q) + i\varepsilon} \langle i, q| T |1, k\rangle \quad (20)$$

$$|\Psi_2\rangle = |\varphi_{2,k}\rangle + \sum_{m,n} |n\rangle R_{nm}(E_2) \langle m| H_{QP} |\varphi_{2,k}\rangle + \sum_{q,i} \frac{|\varphi_{i,q}\rangle}{E_2(k) - E_i(q) + i\varepsilon} \langle i, q| T |2, k\rangle \quad (21)$$

From (20), (21) we obtain the photon wavefunctions in the configuration space $\langle x|\Psi_1\rangle$ and $\langle x|\Psi_2\rangle$:

$$\langle x|\Psi_1\rangle = e^{ikx} |\varphi_1\rangle - i\Gamma e^{ik|x|} t_{11} |\varphi_1\rangle - i\Gamma e^{i(k+k_R)|x|} t_{21} |\varphi_2\rangle \quad (22)$$

$$\langle x|\Psi_2\rangle = e^{ikx} |\varphi_2\rangle - i\Gamma e^{ik|x|} t_{22} |\varphi_2\rangle - i\Gamma e^{i(k-k_R)|x|} t_{12} |\varphi_1\rangle \quad (23)$$

where $k_R = \Omega_R^{(N-1)}/v_g$.

The quantities t_{ij} , $i, j = 1, 2$ are the probability amplitudes for the spontaneous transitions between the levels of two Rabi doublets (see Fig.2). They are related to the transmission matrix as follows: $\langle j, k' | T | i, k \rangle = \langle \varphi_j | T | \varphi_i \rangle \equiv \xi^2 t_{j,i}$. The calculations, the details of which are given in the Appendix D, yield the following expressions for the probability amplitudes:

$$t_{11} = \frac{1}{4\Omega_R^{(N-1)} D(E_1)} \times \left[N(\Omega_R^{(N-1)} + \Delta) (2\delta + \Delta + \Omega_R^{(N-1)}) \right. \\ \left. + (N-1)(\Omega_R^{(N-1)} - \Delta) (2\delta - \Delta + \Omega_R^{(N-1)}) \right. \\ \left. + 4jN(N-1)\Omega_R^{(N-1)}\Gamma + 8\lambda^2 N(N-1) \right] \quad (24)$$

$$t_{21} = -\frac{\lambda\sqrt{N-1}}{2\Omega_R^{(N-1)} D(E_1)} (2\delta + \Omega_R^{(N-1)} - \Delta) \quad (25)$$

$$t_{22} = \frac{1}{4\Omega_R^{(N-1)} D(E_2)} \left[\begin{aligned} & \times \left[N(\Omega_R^{(N-1)} - \Delta) (2\delta + \Delta - \Omega_R^{(N-1)}) \right. \\ & + (N-1)(\Omega_R^{(N-1)} + \Delta) (2\delta - \Omega_R^{(N-1)} - \Delta) \\ & \left. + 4jN(N-1)\Omega_R^{(N-1)}\Gamma - 8\lambda^2N(N-1) \right] \end{aligned} \right] \quad (26)$$

$$t_{12} = -\frac{\lambda\sqrt{N-1}}{2\Omega_R^{(N-1)} D(E_2)} (2\delta - \Omega_R^{(N-1)} - \Delta) \quad (27)$$

The equations (22) and (23) are the main results of our paper. They have a clear physical sense. The transmission signal (at $x > 0$) consists of four waves: two elastic scattering waves with transmission factors $T_{11} = 1 - i\Gamma t_{11}$, $T_{22} = 1 - i\Gamma t_{22}$, and two inelastic scattering waves with transmission factors $T_{12} = -i\Gamma t_{12}$, $T_{21} = -i\Gamma t_{21}$. Accordingly, for reflection waves (at $x < 0$) we have $R_{ij} = -i\Gamma t_{ij}$.

For every initial state the system was before the scattering there are two ways for incoming photon to be scattered (see Fig.3). This is seen in Eqs. (22) and (23) where the every scattering route is a superposition of two final states $|\varphi_1\rangle$ and $|\varphi_2\rangle$. The probability amplitudes t_{11} (24), t_{21} (25) correspond to the channels A and C in Fig.3, and the amplitudes t_{22} (26), t_{12} (27) correspond to the channels B and D , respectively.

We can show by the direct calculation that there exists an exact condition:

$$|T_{ii}|^2 + |1 - T_{ii}|^2 + 2|T_{ji}|^2 = 1 \quad (28)$$

where $i, j = 1, 2$ and $i \neq j$ in third term in l.h.s. of (28). The left hand side of (28) is a sum of transmitted and reflected waves for every route shown in (22) and (23). It is tempting to consider the equation (28) as a condition of the energy flux conservation. However, in our case, as is seen from (22) and (23), the energies of the input and output photons may be different. The condition (28) reflects the conservation of probability: after the scattering the system must be definitely in one of the states, $|\varphi_1\rangle$ or $|\varphi_2\rangle$.

Since for every route (22) or (23) there are two outgoing photons with different frequencies we can measure separately all transmission T_{ij} (or reflection R_{ij}) amplitudes.

VI. TRANSMISSION SPECTRA

As is well known the classical Mollow fluorescent spectrum consists of three lines. However, if the number of cavity photons is small the distance between the Rabi levels in neighbor Rabi doublets is not equal to each other: $\Omega_R^{(N)} > \Omega_R^{(N-1)}$. In this case the fluorescent spectrum for two adjacent doublets will consist of four spectral lines. These lines correspond to the spontaneous transitions between states

(see Fig.2). $|\chi_2\rangle \rightarrow |\varphi_1\rangle$, $|\chi_2\rangle \rightarrow |\varphi_2\rangle$, $|\chi_1\rangle \rightarrow |\varphi_1\rangle$, $|\chi_1\rangle \rightarrow |\varphi_2\rangle$ with the corresponding frequencies of emitting photons: $\omega_c - \frac{1}{2}(\Omega_R^N + \Omega_R^{N-1})$, $\omega_c - \frac{1}{2}(\Omega_R^N - \Omega_R^{N-1})$, $\omega_c + \frac{1}{2}(\Omega_R^N - \Omega_R^{N-1})$, $\omega_c + \frac{1}{2}(\Omega_R^N + \Omega_R^{N-1})$.

The result of our study shows that we obtain the same frequencies for transmitted photons when studying the scattering of a single photon in 1D geometry via the system shown in Fig.1. In addition, we obtained the probability amplitudes (expressions (24), (25), (26), (27)) for spontaneous transitions between levels of two Rabi doublets (see Fig.2). Below we illustrate the application of our results to the transmission spectra for $N = 2$ for strong resonance coupling when the distance between Rabi levels within N manifold are given by $\Omega_R^{(N)}$ (10).

Having in mind to study the effects of adding to a cavity one extra photon we find the transmission and reflection factors for $N = 1$ where we have either one photon in a waveguide and no photon in a cavity with a qubit being in its ground state or no photons in a waveguide and one photon in a cavity. In this case, as is seen from (24)-(26) the only quantity which is different from zero is t_{11} , so that for transmission and reflection we obtain:

$$T_{11}^{(N=1)} = \frac{(\omega - \omega_+) (\omega - \omega_-)}{(\omega - \omega_+) (\omega - \omega_-) + j\Gamma (\omega - \Omega)} \quad (29)$$

$$R_{11}^{(N=1)} = \frac{-j\Gamma (\omega - \Omega)}{(\omega - \omega_+) (\omega - \omega_-) + j\Gamma (\omega - \Omega)} \quad (30)$$

where

$$\omega_{\pm} = \frac{1}{2} (\omega_c + \Omega) \pm \frac{1}{2} \Omega_R^{(1)} \quad (31)$$

The expressions (29) and (30) coincide with those known from the literature [24]. We have here two resonances at the frequencies ω_{\pm} with the distance between them being equal to Rabi frequency $\Omega_R^{(1)}$.

If we add one extra photon to the system we will also have two resonances for every route (22) or (23). But the picture is drastically different from the $N = 1$ case. For example, if before scattering the system is in $|\varphi_1\rangle$ state, then each of the amplitudes t_{11} and t_{21} in (22) has two resonances at the same frequencies. The first resonance at $\omega_c - \frac{1}{2}(\Omega_R^{(2)} + \Omega_R^{(1)})$ corresponds to the transition from the state $|\varphi_1\rangle$ to the state $|\chi_2\rangle$ which subsequently decays either to the initial state $|\varphi_1\rangle$ (the probability of this process is given by the amplitude t_{11} in (22)) or to the state $|\varphi_2\rangle$ with the probability being given by the amplitude t_{21} . The second resonance at $\omega_c + \frac{1}{2}(\Omega_R^{(2)} - \Omega_R^{(1)})$ corresponds to the transition from the state $|\varphi_1\rangle$ to the state $|\chi_1\rangle$ which subsequently decays either to the initial state $|\varphi_1\rangle$ with the probability t_{11} or to the state $|\varphi_2\rangle$ with the probability t_{21} . Therefore, we see that each resonance corresponds to two outgoing photons: the frequency of the first photon is equal to the input frequency, the frequency of the second photon is increased as compared with the first one by the amount $\Omega_R^{(1)}$. Since the frequencies of these two

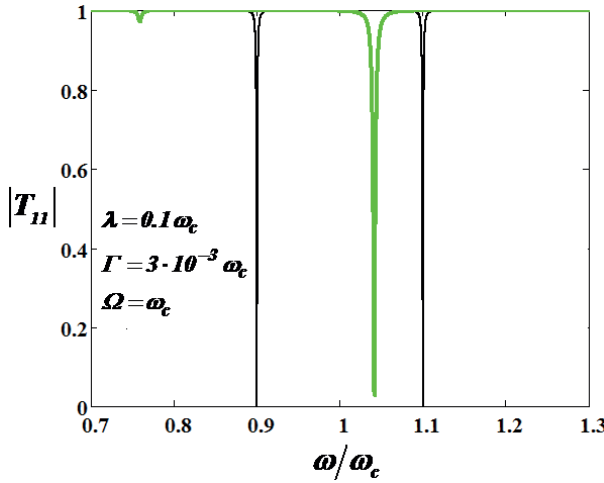


FIG. 9: (Color online) Comparison of transmissions T_{11} for $N = 1$ (black, thin line) and $N = 2$ (green, thick line) for strong resonant coupling.

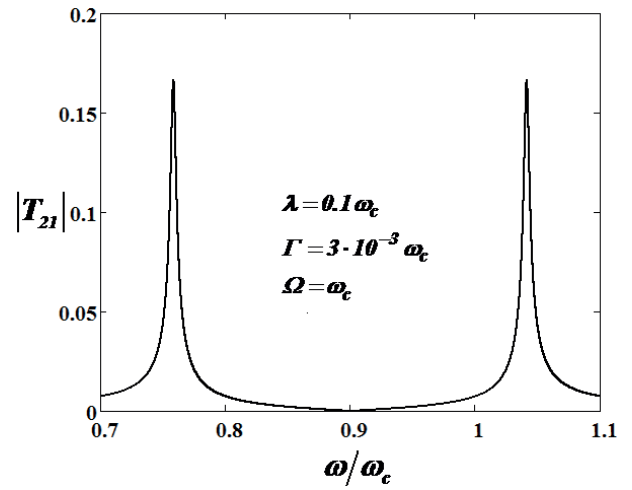


FIG. 10: Inelastic transmission spectrum for $N = 2$ and strong resonant coupling after the excitation of $|\varphi_1\rangle$ state. The outgoing photon leaves the cavity with the increased frequency $\omega + \Omega_R^{(1)}$.

photons are different, they can be detected separately and independently of each other.

In Fig.9 we compare the transmission coefficients T_{11} for $N = 1$ and $N = 2$ as a function of the frequency of incident photon for the case of strong resonant coupling: $\lambda \gg \Gamma, \omega_C = \Omega$. Two dips which are symmetric relative to ω_C are calculated from expression (29). These dips are located at $\omega_C \pm \Omega_R^{(1)}$. The addition of one extra photon gives rise to the appearance of two dips, which results from the excitation of the level $|\varphi_1\rangle$. These dips are calculated from (24). A shallow dip, which is located at the frequency $\omega_c - \frac{1}{2}(\Omega_R^{(2)} + \Omega_R^{(1)})$ corresponds to the transition $|\varphi_1\rangle \rightarrow |\chi_2\rangle \rightarrow |\varphi_1\rangle$, while a deep dip, which is located at the frequency $\omega_c + \frac{1}{2}(\Omega_R^{(2)} - \Omega_R^{(1)})$ corresponds to the transition $|\varphi_1\rangle \rightarrow |\chi_1\rangle \rightarrow |\varphi_1\rangle$. The distance between two dips is equal to $\Omega_R^{(2)}$. For both cases the frequency of outgoing photons is equal to the frequency of the input photon.

In Fig.10 we show the transmission spectrum which is given by the amplitude t_{21} in (22). Here the resonance points are the same as those in Fig.9, however, the outgoing photon has the increased frequency $\omega + \Omega_R^{(1)}$. After the scattering the cavity is being left in the state $|\varphi_2\rangle$. The left peak in Fig.10 corresponds to transitions $|\varphi_1\rangle \rightarrow |\chi_2\rangle \rightarrow |\varphi_2\rangle$ with the frequency of outgoing photon $\omega = \omega_c - \frac{1}{2}(\Omega_R^{(2)} - \Omega_R^{(1)})$. The right peak corresponds to transitions $|\varphi_1\rangle \rightarrow |\chi_1\rangle \rightarrow |\varphi_2\rangle$ with the frequency of outgoing photon $\omega = \omega_c + \frac{1}{2}(\Omega_R^{(2)} + \Omega_R^{(1)})$.

If initially the system is in the state $|\varphi_2\rangle$, the scattering wave function is given by (23). The resonance points are being shifted on the frequency axis to the right by $\Omega_R^{(1)}$. The first resonance at $\omega_c - \frac{1}{2}(\Omega_R^{(2)} - \Omega_R^{(1)})$ corresponds to the transition $|\varphi_2\rangle \rightarrow |\chi_2\rangle$ while the second one at $\omega_c + \frac{1}{2}(\Omega_R^{(2)} + \Omega_R^{(1)})$ corresponds to the transition $|\varphi_2\rangle \rightarrow |\chi_1\rangle$. Each of these excitations then decays either to the initial state $|\varphi_2\rangle$ with the probability amplitude t_{22} or to the state $|\varphi_1\rangle$ with the probability amplitude t_{12} . The transmission spectrum for $N = 2$ for the case when the system is left after scattering in the

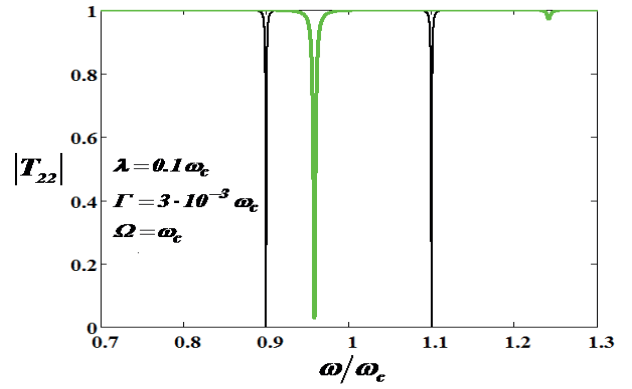


FIG. 11: (Color online) Comparison of transmissions T_{11} for $N = 1$ (black, thin line) and T_{22} for $N = 2$ (green, thick line) for strong resonant coupling.

state $|\varphi_2\rangle$ is shown in Fig.11. This picture is similar to that shown in Fig.9. A deep dip, which is located at the frequency $\omega_c - \frac{1}{2}(\Omega_R^{(2)} - \Omega_R^{(1)})$ corresponds to the transition $|\varphi_2\rangle \rightarrow |\chi_2\rangle \rightarrow |\varphi_2\rangle$, while a shallow dip, which is located at the frequency $\omega_c + \frac{1}{2}(\Omega_R^{(2)} + \Omega_R^{(1)})$ corresponds to the transition $|\varphi_2\rangle \rightarrow |\chi_1\rangle \rightarrow |\varphi_2\rangle$. The distance between two dips is equal to $\Omega_R^{(2)}$. For both cases the frequency of outgoing photons is equal to the frequency of the input photon.

In Fig.12 we show in one plot the transmission spectra which are given by the amplitudes t_{21} in (22) and t_{12} in (23). The black thin lines show the transmission spectrum when the system was initially in the state $|\varphi_1\rangle$ and after scattering was left in the state $|\varphi_2\rangle$ with the outgoing photon with the frequency increased by $\Omega_R^{(1)}$. These spectrum is the same as is shown in Fig.10. The green thick lines in Fig.12 show the transmission spectrum when the system was initially in the state $|\varphi_2\rangle$ and after scattering was left in the state $|\varphi_1\rangle$ with the outgoing photon with the frequency reduced by

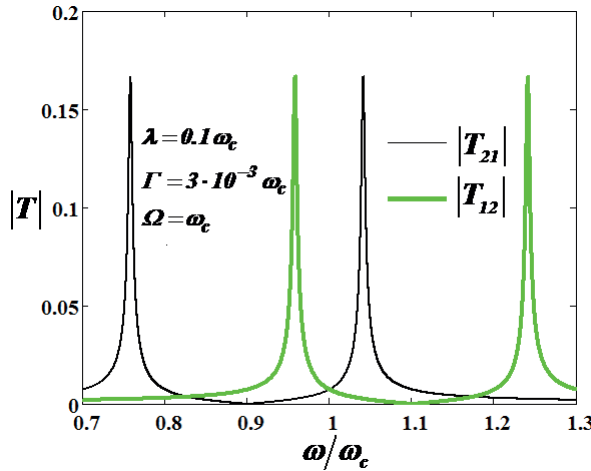


FIG. 12: Color on line. Inelastic transmission spectra for $N = 2$ and strong resonant coupling after the excitation of the state $|\varphi_1\rangle$ (thin, black line) and the state $|\varphi_2\rangle$ (thick, green line).

$\Omega_R^{(1)}$. The left peak of this spectrum corresponds to the excitation of the transition $|\varphi_2\rangle \rightarrow |\chi_2\rangle$ at the frequency of ingoing photon $\omega_c - \frac{1}{2}(\Omega_R^{(2)} - \Omega_R^{(1)})$. The state $|\chi_2\rangle$ then decays to the state $|\varphi_1\rangle$ with the frequency of outgoing photon $\omega_c - \frac{1}{2}(\Omega_R^{(2)} + \Omega_R^{(1)})$. The right peak corresponds to the excitation of the transition $|\varphi_2\rangle \rightarrow |\chi_1\rangle$ by the ingoing photon with the frequency $\omega_c + \frac{1}{2}(\Omega_R^{(2)} + \Omega_R^{(1)})$. The state $|\chi_1\rangle$ then decays to the state $|\varphi_1\rangle$ with the frequency of outgoing photon $\omega_c + \frac{1}{2}(\Omega_R^{(2)} - \Omega_R^{(1)})$.

VII. CONCLUSION

We develop a theoretical method for the calculation of a microwave transport in 1D waveguide side coupled to a resonant N -photon cavity with embedded artificial atom (qubit). The method is based on the projection operator formalism and a non-Hermitian Hamiltonian approach, which enables us to obtain the analytical expressions for the probability amplitudes of spontaneous transitions between the dressed levels of adjacent doublets in N -photon cavity. We considered in detail a single photon transport for the cavity with two photons. We show that if the number of the cavity photons is small the transmitted and reflected spectra reveal a quadruplet structure with two central peaks and two sidebands. This is the direct manifestation of the quantum nature of light which results in a different space between the levels in adjacent Rabi doublets. As the number of the cavity photons is increased the two central peaks merge giving a classical Mollow triplet.

The results obtained in the paper can be applied for the investigation of microwave photon transport in superconducting circuits with embedded superconducting qubits based on Josephson junctions[1, 5]. The specific properties of the qubit are encoded in only two parameters: the qubit energy Ω and its coupling to the cavity λ . For example, for a superconducting qubit $\Omega = \sqrt{\varepsilon^2 + \Delta^2}$ where $\varepsilon = \frac{2I_q}{\hbar}(\Phi_x - \Phi_0/2)$

is an external parameter which by virtue of external magnetic flux, Φ_x controls the gap between ground and excited states [27], I_q is a persistent current along a qubit loop, $\Phi_0 = h/2e$ is a flux quantum. The quantity Δ is the qubit's gap at the degeneracy point ($\varepsilon = 0$). The coupling strength $\lambda = g\Delta/\Omega$ [23], where g is the qubit-cavity coupling at the degeneracy point. For a charge qubit $\Omega = \sqrt{\varepsilon_J^2 + \varepsilon_C^2}$ where $\varepsilon_J = 2E_J|\cos(\pi\Phi_x/\Phi_0)|$, $\varepsilon_C = 4E_C(1 - 2n_g)$, where E_J is a coupling energy of Josephson junction, E_C is a charging energy, n_g is a dimensionless gate charge which can be tuned by applying the voltage V_g to the gate capacitance C_g : $n_g = C_g V_g / e$ [28].

ACKNOWLEDGMENTS

The authors are grateful to E. Il'ichev for useful discussions. This work has been supported by the Russian Science Foundation under grant No.16-19-10069.

Appendix A: The calculation of H_{XY}

With the aid of explicit expressions (11) and (12) for Q and P we obtain for the parts H_{XY} of the full Hamiltonian (5) the following expressions:

$$H_{QQ} = \frac{1}{2}\hbar\Omega|2\rangle\langle 2| - \frac{1}{2}\hbar\Omega|1\rangle\langle 1| + \hbar\omega_c(N-1)|2\rangle\langle 2| + \hbar\lambda\sqrt{N}|1\rangle\langle 2| + \hbar\lambda\sqrt{N}|2\rangle\langle 1| + \hbar\omega_cN|1\rangle\langle 1| \quad (A1)$$

$$H_{PP} = \frac{1}{2}\hbar\Omega\sum_k|k_2\rangle\langle k_2| + \hbar\omega_c(N-1)\sum_k|k_1\rangle\langle k_1| + \hbar\lambda\sqrt{N-1}\sum_k|k_1\rangle\langle k_2| + \hbar\lambda\sqrt{N-1}\sum_k|k_2\rangle\langle k_1| + \sum_k\hbar\omega_k|k_1\rangle\langle k_1| + \sum_k\hbar\omega_k|k_2\rangle\langle k_2| + \hbar\omega_c(N-2)\sum_k|k_2\rangle\langle k_2| - \frac{1}{2}\hbar\Omega\sum_k|k_1\rangle\langle k_1| \quad (A2)$$

$$H_{PQ} = \hbar\xi\sqrt{N-1}\sum_k|k_2\rangle\langle 2| + \hbar\xi\sqrt{N}\sum_k|k_1\rangle\langle 1| \quad (A3)$$

$$H_{QP} = \hbar\xi\sqrt{N}\sum_k|1\rangle\langle k_1| + \hbar\xi\sqrt{N-1}\sum_k|2\rangle\langle k_2| \quad (A4)$$

Appendix B: Calculation of the effective Hamiltonian

From (2) we find the matrix elements of effective hamiltonian in Q subspace.

$$\begin{aligned} \langle m | H_{eff} | n \rangle &= \langle m | H_{QQ} | n \rangle \\ &+ \sum_{\substack{i,j=1 \\ k,k'}}^2 \langle m | H_{QP} | \varphi_{i,k} \rangle \langle \varphi_{i,k} | \frac{1}{E - H_{PP} + i\varepsilon} | \varphi_{j,k'} \rangle \langle \varphi_{j,k'} | H_{PQ} | n \rangle \\ &= \langle m | H_{QQ} | n \rangle + \sum_{i=1,k}^{i=2} \frac{\langle m | H_{QP} | \varphi_{i,k} \rangle \langle \varphi_{i,k} | H_{PQ} | n \rangle}{E - E_i(k) + i\varepsilon} \end{aligned} \quad (B1)$$

Fortunately, the matrix elements $\langle m | H_{QP} | \varphi_{i,k} \rangle$ and $\langle \varphi_{i,k} | H_{PQ} | n \rangle$ do not depend on the photon momentum k . The direct calculations yield:

$$\langle 1 | H_{QP} | \varphi_{1,k} \rangle = a_1 \xi \sqrt{N}, \quad \langle 2 | H_{QP} | \varphi_{1,k} \rangle = b_1 \xi \sqrt{N-1} \quad (B2)$$

$$\langle 1 | H_{QP} | \varphi_{2,k} \rangle = a_2 \xi \sqrt{N}, \quad \langle 2 | H_{QP} | \varphi_{2,k} \rangle = b_2 \xi \sqrt{N-1} \quad (B3)$$

With the use of (A1) and (B2), (B3) we obtain for the matrix elements of (B1):

$$\langle 1 | H_{eff} | 1 \rangle = \omega_C N - \frac{1}{2} \Omega + a_1^2 \xi^2 N J_1(E) + a_2^2 \xi^2 N J_2(E) \quad (B4a)$$

$$\begin{aligned} \langle 2 | H_{eff} | 2 \rangle &= \omega_C (N-1) + \frac{1}{2} \Omega + b_1^2 \xi^2 (N-1) J_1(E) \\ &+ b_2^2 \xi^2 (N-1) J_2(E) \end{aligned} \quad (B4b)$$

$$\begin{aligned} \langle 1 | H_{eff} | 2 \rangle &= \langle 2 | H_{eff} | 1 \rangle = \lambda \sqrt{N} \\ &+ a_1 b_1 \xi^2 \sqrt{N(N-1)} J_1(E) + a_2 b_2 \xi^2 \sqrt{N(N-1)} J_2(E) \end{aligned} \quad (B4c)$$

where

$$J_j(E) = \sum_k \frac{1}{E - E_j(k) + i\varepsilon} = \frac{L}{2\pi} \int \frac{dk}{E - E_j(k) + i\varepsilon} \quad (B5)$$

It will be shown below that all quantities $J_j(E)$ in (B4a), (B4b), and (B4c) are the same and do not depend on the running energy E .

$$J_j(E) = -\frac{2\pi i}{v_g} \quad (B6)$$

where v_g is the velocity of microwave photons in a waveguide.

Finally, with the use of properties of coefficients a_i, b_i from in (9): $a_1^2 + a_2^2 = 1, b_1^2 + b_2^2 = 1, a_1 b_1 + a_2 b_2 = 0$ we obtain for the matrix elements of H_{eff} the following expressions:

$$\langle 1 | H_{eff} | 1 \rangle = \omega_C N - \frac{1}{2} \Omega - j N \Gamma \quad (B7a)$$

$$\langle 2 | H_{eff} | 2 \rangle = \omega_C (N-1) + \frac{1}{2} \Omega - j (N-1) \Gamma \quad (B7b)$$

$$\langle 1 | H_{eff} | 2 \rangle = \langle 2 | H_{eff} | 1 \rangle = \lambda \sqrt{N} \quad (B7c)$$

where we introduce the width of the cavity decay rate $\Gamma = L \xi^2 / v_g$.

Appendix C: Calculation of the matrix R

Here we calculate the matrix $R_{m,n}(E)$ which is the matrix inverse of the matrix $\langle m | (E - H_{eff}) | n \rangle$:

$$R_{n,m}(E) = \langle n | \frac{1}{E - H_{eff}} | m \rangle \quad (C1)$$

From (B7a), (B7b), (B7c) we find the elements of R matrix (C1).

$$R_{11}(E) = \frac{1}{D(E)} \left(E - \omega_C (N-1) - \frac{1}{2} \Omega + j (N-1) \Gamma \right) \quad (C2a)$$

$$R_{22}(E) = \frac{1}{D(E)} \left(E - \omega_C N + \frac{1}{2} \Omega + j N \Gamma \right) \quad (C2b)$$

$$R_{12}(E) = R_{21}(E) = \frac{\lambda \sqrt{N}}{D(E)} \quad (C2c)$$

where $D(E)$ is given in (16).

Appendix D: Calculation of transmission matrix (19)

As was shown in Sec.V, $\langle j, k' | T | i, k \rangle = \langle \varphi_j | T | \varphi_i \rangle \equiv \xi^2 t_{j,i}$. With the aid of (B2), (B3) we obtain for matrix t_{ij} the following expressions:

$$\begin{aligned} t_{11} &= (a_1^2 N R_{11}(E_1) + b_1^2 (N-1) R_{22}(E_1) \\ &+ 2 a_1 b_1 \sqrt{N(N-1)} R_{12}(E_1)) \end{aligned} \quad (D1a)$$

$$\begin{aligned} t_{12} &= (a_1 a_2 N R_{11}(E_1) + b_1 b_2 (N-1) R_{22}(E_1) \\ &+ \sqrt{N(N-1)} (a_2 b_1 + a_1 b_2) R_{12}(E_1)) \end{aligned} \quad (D1b)$$

$$\begin{aligned} t_{22} &= (a_2^2 N R_{11}(E_2) + b_2^2 (N-1) R_{22}(E_2) \\ &+ 2 a_2 b_2 \sqrt{N(N-1)} R_{12}(E_2)) \end{aligned} \quad (D1c)$$

$$t_{21} = (a_1 a_2 N R_{11}(E_2) + b_1 b_2 (N-1) R_{22}(E_2) + \sqrt{N(N-1)} (a_2 b_1 + a_1 b_2) R_{21}(E_2)) \quad (\text{D1d})$$

If we substitute in these expressions a_i, b_i for their explicit forms

$$a_1 = \frac{1}{\sqrt{2}} \sqrt{1 - \frac{\Omega - \omega_c}{\Omega_R^{(N-1)}}} \quad b_1 = \frac{1}{\sqrt{2}} \sqrt{1 + \frac{\Omega - \omega_c}{\Omega_R^{(N-1)}}} \quad (\text{D2})$$

$$a_2 = -\frac{1}{\sqrt{2}} \sqrt{1 + \frac{\Omega - \omega_c}{\Omega_R^{(N-1)}}} \quad b_2 = \frac{1}{\sqrt{2}} \sqrt{1 - \frac{\Omega - \omega_c}{\Omega_R^{(N-1)}}} \quad (\text{D3})$$

and R from (C2a), (C2c), (C2b), we obtain the expressions for t_{ij} given in Sec.V in (24), (27), (26), (25).

Appendix E: Calculation of the photon wavefunction

As we show in the main text, there are two possible initial states (9): $|\varphi_1\rangle$ and $|\varphi_2\rangle$. Accordingly, there are two wavefunctions (4):

$$|\Psi_1\rangle = |\varphi_{1,k}\rangle + \frac{1}{E_1 - H_{eff}} H_{QP} |\varphi_{1,k}\rangle + \frac{1}{E_1 - H_{PP} + i\varepsilon} H_{PQ} \frac{1}{E_1 - H_{eff}} H_{QP} |\varphi_{1,k}\rangle \quad (\text{E1a})$$

$$|\Psi_2\rangle = |\varphi_{2,k}\rangle + \frac{1}{E_2 - H_{eff}} H_{QP} |\varphi_{2,k}\rangle + \frac{1}{E_2 - H_{PP} + i\varepsilon} H_{PQ} \frac{1}{E_2 - H_{eff}} H_{QP} |\varphi_{2,k}\rangle \quad (\text{E1b})$$

Next we use the properties of completeness of P and Q ($P + Q = 1$) and their orthogonality ($PQ = QP = 0$) to obtain from (E1a) and (E1b)

$$|\Psi_1\rangle = |\varphi_{1,k}\rangle + \sum_{n,m=1}^2 |n\rangle \langle n| \frac{1}{E_1 - H_{eff}} |m\rangle \langle m| H_{QP} |\varphi_{1,k}\rangle + \sum_{i,j=1}^2 \left\{ |\varphi_{i,k}\rangle \langle \varphi_{i,k}| \frac{1}{E_1 - H_{PP} + i\varepsilon} |\varphi_{i,k'}\rangle \right. \\ \left. \times \langle \varphi_{j,k'}| H_{PQ} |n\rangle \langle n| \frac{1}{E_1 - H_{eff}} |m\rangle \langle m| H_{QP} |\varphi_{1,k}\rangle \right\} \quad (\text{E2})$$

$$|\Psi_2\rangle = |\varphi_{2,k}\rangle + \sum_{n,m=1}^2 |n\rangle \langle n| \frac{1}{E_2 - H_{eff}} |m\rangle \langle m| H_{QP} |\varphi_{2,k}\rangle + \sum_{i,j=1}^2 \left\{ |\varphi_{i,k}\rangle \langle \varphi_{i,k}| \frac{1}{E_2 - H_{PP} + i\varepsilon} |\varphi_{i,k'}\rangle \right. \\ \left. \times \langle \varphi_{j,k'}| H_{PQ} |n\rangle \langle n| \frac{1}{E_2 - H_{eff}} |m\rangle \langle m| H_{QP} |\varphi_{2,k}\rangle \right\} \quad (\text{E3})$$

From these equations it follows immediately the expressions (20) and (21), which we write here in the following form:

$$|\Psi_1\rangle = |\varphi_{1,k}\rangle + \sum_{m,n} |n\rangle R_{nm}(E_1) \langle m| H_{QP} |\varphi_{1,k}\rangle + \xi^2 \sum_{q,i} \frac{|\varphi_{i,q}\rangle t_{i1}}{E_1(k) - E_i(q) + i\varepsilon} \quad (\text{E4})$$

$$|\Psi_2\rangle = |\varphi_{2,k}\rangle + \sum_{m,n} |n\rangle R_{nm}(E_2) \langle m| H_{QP} |\varphi_{2,k}\rangle + \xi^2 \sum_{q,i} \frac{|\varphi_{i,q}\rangle t_{i2}}{E_2(k) - E_i(q) + i\varepsilon} \quad (\text{E5})$$

In order to obtain photon wavefunction in a configuration space we multiply (E4) and (E5) from the left by bra vector $\langle x|$, and taking into account that $\langle x|n\rangle = 0$, $\langle x|\varphi_{i,k}\rangle = e^{ikx} |\varphi_i\rangle$, we obtain:

$$\langle x|\Psi_1\rangle = e^{ikx} |\varphi_1\rangle + \xi^2 \sum_{i=1}^2 J_{i,1} t_{i1} |\varphi_i\rangle \quad (\text{E6})$$

$$\langle x|\Psi_2\rangle = e^{ikx} |\varphi_2\rangle + \xi^2 \sum_{i=1}^2 J_{i,2} t_{i2} |\varphi_i\rangle \quad (\text{E7})$$

where

$$J_{i,j} = \sum_q \frac{e^{iqx}}{E_j(k) - E_i(q) + i\varepsilon} \quad (\text{E8})$$

Below we calculate the quantities $J_{i,j}$. The result is as follows:

$$J_{11} = J_{22} = -i \frac{L}{v_g} e^{ik|x|} \quad (\text{E9})$$

$$J_{12} = -i \frac{L}{v_g} e^{i(k-k_R)|x|} \quad (\text{E10})$$

$$J_{21} = -i \frac{L}{v_g} e^{i(k+k_R)|x|} \quad (\text{E11})$$

where $k_R = \Omega_R^{(N-1)}/v_g$.

With the account of these results we obtain for the photon wavefunctions (E6), (E7) the expressions (22) and 23) from the main text.

Appendix F: Calculation of $J_{i,j}$

From (14) we find the energy difference in the denominator of (E8):

$$\begin{aligned} E_i(k) - E_i(q) &= \omega_k - \omega_q = v_g(k - q); \\ E_1(k) - E_2(q) &= \omega_k - \omega_q + \Omega_R^{(N-1)} = v_g(k - q + k_R); \\ E_2(k) - E_1(q) &= \omega_k - \omega_q - \Omega_R = v_g(k - q - k_R) \end{aligned} \quad (\text{F1})$$

As an example we calculate below the quantity J_{12} (E10) where we substitute the summation over q for the integration:

$$J_{12} = \frac{L}{2\pi} \int_{-\infty}^{+\infty} \frac{e^{iqx}}{\omega_k - \omega_q - \Omega_R^{(N-1)} + i\varepsilon} dq \quad (\text{F2})$$

The main contribution to this integral comes from the re-

gion where $\omega_q \approx \omega_k - \Omega_R^{(N-1)}$. Since ω_q is the even function of q , it can be approximated away from the cutoff frequency as $\omega_q \equiv v_g|q|$. In this case the poles of the integrand (F2) in the q plane are located near the points $q \approx \pm q_0$ where $q_0 = (k - k_R)$. From denominator in (F2) we see that one pole is located in the upper half of the q plane, $q = q_0 + i\varepsilon$, the other pole is located in the lower half of the q plane, $q = -q_0 - i\varepsilon$. For positive x , when calculating the integral (F2) we must close the path in the upper plane. For negative x the path should be closed in lower plane. Thus, we obtain:

$$J_{12} = -i \frac{L}{\hbar v_g} e^{i(k - k_R)|x|} \quad (\text{F3})$$

The quantities J_{11} , J_{22} (E9) and J_{21} (E11) can be calculated by the same procedure.

[1] J. Q. You and F. Nori, Atomic physics and quantum optics using superconducting circuits. *Nature* **474**, 589 (2011).

[2] S. M. Girvin, M. H. Devoret and R. J. Schoelkopf, Circuit QED and engineering charge-based superconducting qubits. *Physica Scripta* **T137**, 014012 (2009).

[3] Y. A. Pashkin, O. Astafiev, T. Yamamoto, Y. Nakamura and J. S. Tsai, Josephson charge qubits: a brief review. *Quantum Information Processing* **8**, 55 (2009).

[4] B. C. Sanders, Quantum optics in superconducting circuits. AIP Conference Proceedings **1398**, 46 (2011).

[5] A. Wallraff, D. I. Schuster, A. Blais, L. Frunzio, R.-S. Huang, J. Majer, S. Kumar, S. M. Girvin, and R. J. Schoelkopf, Strong coupling of a single photon to a superconducting qubit using circuit quantum electrodynamics. *Nature*, **431**, 162 (2004).

[6] T. Niemczyk, F. Deppe, H. Huebl, E. P. Menzel, F. Hocke, M. J. Schwarz, J. J. Garcia-Ripoll, D. Zueco, T. Hummer, E. Solano, A. Marx and R. Gros, Circuit quantum electrodynamics in the ultrastrong-coupling regime. *Nature Physics* **6**, 772 (2010).

[7] S. Rebic, J. Twamley and G. J. Milburn, Giant Kerr Nonlinearities in Circuit Quantum Electrodynamics. *Phys. Rev. Lett.* **103**, 150503 (2009).

[8] M. Rehak, P. Neilinger, M. Grajcar, G. Oelsner, U. Hübner, E. Il'ichev, and H.-G. Meyer, Parametric amplification by coupled flux qubits. *Appl. Phys. Lett.* **104**, 162604 (2014).

[9] H.-C. Sun, Yu-xi Liu, H. Ian, J. Q. You, E. Il'ichev, and Franco Nori, Electromagnetically induced transparency and Autler-Townes splitting in superconducting flux quantum circuits. *Phys. Rev. A* **89**, 063822 (2014).

[10] A. A. Abdumalikov, Jr., O. Astafiev, A. M. Zagoskin, Yu. A. Pashkin, Y. Nakamura and J. S. Tsai, Electromagnetically Induced Transparency on a Single Artificial Atom. *Phys. Rev. Lett.* **104**, 193601 (2010).

[11] J. Joo, J. Bourassa, A. Blais and B. C. Sanders, Electromagnetically Induced Transparency with Amplification in Superconducting Circuits. *Phys. Rev. Lett.* **105**, 073601 (2010).

[12] Hai-Chao Li and Guo-Qin Ge, Electromagnetically Induced Transparency Using a Artificial Molecule in Circuit Quantum Electrodynamics. *Optics and Photonics Journal* **3**, 29 (2013).

[13] M. Baur, S. Filipp, R. Bianchetti, J. M. Fink, M. Göppl, L. Steffen, P. J. Leek, A. Blais, and A. Wallraff, Measurement of Autler-Townes and Mollow Transitions in a Strongly Driven Superconducting Qubit. *Phys. Rev. Lett.* **102**, 243602 (2009).

[14] O. Astafiev, A. M. Zagoskin, A. A. Abdumalikov Jr., Yu. A. Pashkin, T. Yamamoto, K. Inomata, Y. Nakamura, J. S. Tsai, Resonance Fluorescence of a Single Artificial Atom. *Science*, **327**, 840 (2010).

[15] Io-Chun Hoi, T. Palomaki, J. Lindkvist, G. Johansson, P. Delsing, and C. M. Wilson, Generation of nonclassical microwave states using an artificial atom in 1D open space. *Phys. Rev. Lett.* **108**, 263601 (2012).

[16] C. Lang, D. Bozyigit, C. Eichler, L. Steffen, J. M. Fink, A. A. Abdumalikov, Jr., M. Baur, S. Filipp, M. P. da Silva, A. Blais, and A. Wallraff, Observation of Resonant Photon Blockade at Microwave Frequencies Using Correlation Function Measurements. *Phys. Rev. Lett.* **106** 243601 (2011).

[17] D. M. Toyli, A. W. Eddins, S. Boutin, S. Puri, D. Hover, V. Bolkhovsky, W. D. Oliver, A. Blais, and I. Siddiqi, Resonance Fluorescence from an Artificial Atom in Squeezed Vacuum. *Phys. Rev. X* **6**, 031004 (2016).

[18] M. A. Sillanpää, J. Li, K. Cicak, F. Altomare, J. I. Park, R. W. Simmonds, G. S. Paraoanu, and P. J. Hakonen, Autler-Townes Effect in a Superconducting Three-Level System. *Phys. Rev. Lett.* **103**, 193601 (2009).

[19] B. R. Mollow, Power Spectrum of light scattered by three level systems. *Phys. Rev.* **188**, 1969 (1969).

[20] J. M. Fink, M. Göppl, M. Baur, R. Bianchetti, P. J. Leek, A. Blais, and A. Wallraff, Climbing the Jaynes-Cummings ladder and observing its \sqrt{n} nonlinearity in a cavity QED system. *Nature* **454**, 315 (2008).

[21] N. Auerbach and V. Zelevinsky, Super-radiant dynamics, doorways, and resonances in nuclei and other open mesoscopic systems. *Rep. Prog. Phys.* **74**, 106301 (2011).

[22] Ya. S. Greenberg and A. A. Shtygashev, Non hermitian Hamiltonian approach to the microwave transmission through a one-dimensional qubit chain. *Phys. Rev. A* **92**, 063835 (2015).

[23] A. N. Omelyanchouk, S. N. Shevchenko, Ya. S. Greenberg, O. Astafiev, and E. Il'ichev, Quantum behavior of a flux qubit coupled to a resonator. *Low Temp. Phys.* **36**, 893 (2010).

[24] Jung-Tsung Shen and Shanhui Fan, Theory of single-photon transport in a single-mode waveguide. I. Coupling to a cavity

containing a two-level atom. *Phys. Rev. A* **79**, 023837 (2009)

[25] R. Bianchetti, S. Filipp, M. Baur, J. M. Fink, M. Göppl, P. J. Leek, L. Steffen, A. Blais, and A. Wallraff, Dynamics of dispersive single-qubit readout in circuit quantum electrodynamics. *Phys. Rev. A* **80**, 043840 (2009).

[26] I. Rotter, Dynamics of quantum systems. *Phys. Rev. E* **64**, 036213(2001).

[27] Caspar H. van der Wal, A. C. J. ter Haar, F. K. Wilhelm, R. N. Schouten, C. J. P. M. Harmans, T. P. Orlando, Seth Lloyd, and J. E. Mooij, Quantum Superposition of Macroscopic Persistent-Current States. *Science* **290**, 773 (2000).

[28] A. Blais, Ren-Shou Huang, A. Wallraff, S. M. Girvin, and R. J. Schoelkopf, Cavity quantum electrodynamics for superconducting electrical circuits: an architecture for quantum computation. *Phys. Rev. A* **69**, 062320 (2004).